

DOI: 10.1002/cmdc.201200480

A Combination Strategy to Inhibit Pim-1: Synergism between Noncompetitive and ATP-Competitive Inhibitors

Mattia Mori,^[a, b] Cristina Tintori,^[a] Robert Selwyne Arul Christopher,^[a] Marco Radi,^[a] Silvia Schenone,^{*,[c]} Francesca Musumeci,^[c] Chiara Brullo,^[c] Patrizia Sanità,^[d] Simona Delle Monache,^[d] Adriano Angelucci,^[d] Miroslava Kissova,^[e] Emmanuele Crespan,^[e] Giovanni Maga,^[e] and Maurizio Botta^{*,[a, f]}

Pim-1 is a serine/threonine kinase critically involved in the initiation and progression of various types of cancer, especially leukemia, lymphomas and solid tumors such as prostate, pancreas and colon, and is considered a potential drug target against these malignancies. In an effort to discover new potent Pim-1 inhibitors, a previously identified ATP-competitive indolyl-pyrrolone scaffold was expanded to derive structure–activity relationship data. A virtual screening campaign was also performed, which led to the discovery of additional ATP-competitive inhibitors as well as a series of 2-aminothiazole derivatives, which are noncompetitive with respect to both ATP and peptide substrate. This mechanism of action, which resembles allosteric inhibition, has not previously been characterized for

Pim-1. Notably, further evaluation of the 2-aminothiazoles indicated a synergistic inhibitory effect in enzymatic assays when tested in combination with ATP-competitive inhibitors. A synergistic effect in the inhibition of cell proliferation by ATP-competitive and ATP-noncompetitive compounds was also observed in prostate cancer cell lines (PC3), where all Pim-1 inhibitors tested in showed synergism with the known anticancer agent, paclitaxel. These results further establish Pim-1 as a target in cancer therapy, and highlight the potential of these agents for use as adjuvant agents in the treatment of cancer diseases in which Pim-1 is associated with chemotherapeutic resistance.

Introduction

Proviral integration site for Moloney murine leukemia virus 1 (*PIM1*) is a proto-oncogene first identified as a preferential proviral integration site in Moloney murine leukemia virus-induced T-cell lymphomas.^[1,2] *PIM1* encodes the serine/threonine kinase Pim-1, the first member described of a family that includes at least two other kinases, Pim-2 and Pim-3, which are structurally related to Pim-1.^[2,3]

Human Pim-1 is a 313-amino acid serine/threonine kinase that possesses several biological functions in cell survival, proliferation and differentiation, and its overexpression has been observed in several human cancers.^[4,5] Indeed, the gene that encodes Pim-1 is a proto-oncogene implicated in early cell

transformation and tumor progression, especially in hematopoietic malignancies and prostate carcinoma where it is a marker of a poor prognosis.^[6–11] Somatic mutations and chromosomal translocations in *PIM1* have been also identified in primary central nervous system (CNS) lymphomas.^[12] In addition, overexpression of Pim-1 in hemopoietic cells enhances cell survival by protecting these cells from apoptosis induced by cytokine withdrawal, glucocorticoids, and genotoxic stress. In light of its oncogenic potential, Pim-1 is emerging as an important new target for drug discovery. Accordingly, research into Pim-1 inhibitors has received growing attention in recent years and has led to the discovery of small molecules charac-

[a] Dr. M. Mori,⁺ Dr. C. Tintori,⁺ Dr. R. S. A. Christopher, Dr. M. Radi, Prof. M. Botta
Dipartimento di Biotecnologie, Chimica e Farmacia
Università degli Studi di Siena
Via A. Moro 2, 53100 Siena (Italy)
E-mail: botta.maurizio@gmail.com

[b] Dr. M. Mori⁺
Dipartimento di Chimica e Tecnologie del Farmaco
Università di Roma "La Sapienza"
Piazzale A. Moro 5, 00185 Roma (Italy)

[c] Prof. S. Schenone, Dr. F. Musumeci, Dr. C. Brullo
Dipartimento di Farmacia
Sezione di Chimica del Farmaco e del Prodotto Cosmetico
University of Genoa
Viale Benedetto XV 3, 16132 Genova (Italy)
E-mail: schensil@unige.it

[d] Dr. P. Sanità, Dr. S. Delle Monache, Dr. A. Angelucci
Dipartimento di Scienze Cliniche Applicate e Biotecnologiche
Università dell'Aquila
Via Vetoio (Coppito 2), 67100 Coppito, L'Aquila (Italy)

[e] M. Kissova, Dr. E. Crespan, Dr. G. Maga
Istituto di Genetica Molecolare (IGM-CNR)
Via Abbiategrasso 207, 27100 Pavia (Italy)

[f] Prof. M. Botta
Sbarro Institute for Cancer Research and Molecular Medicine
Center for Biotechnology, College of Science and Technology
Temple University
BioLife Science Building, Suite 333, 1900 N 12th St., Philadelphia, PA 19122 (USA)

[*] Authors equally contributed to this work.

 Supporting information for this article is available on the WWW under <http://dx.doi.org/10.1002/cmdc.201200480>.

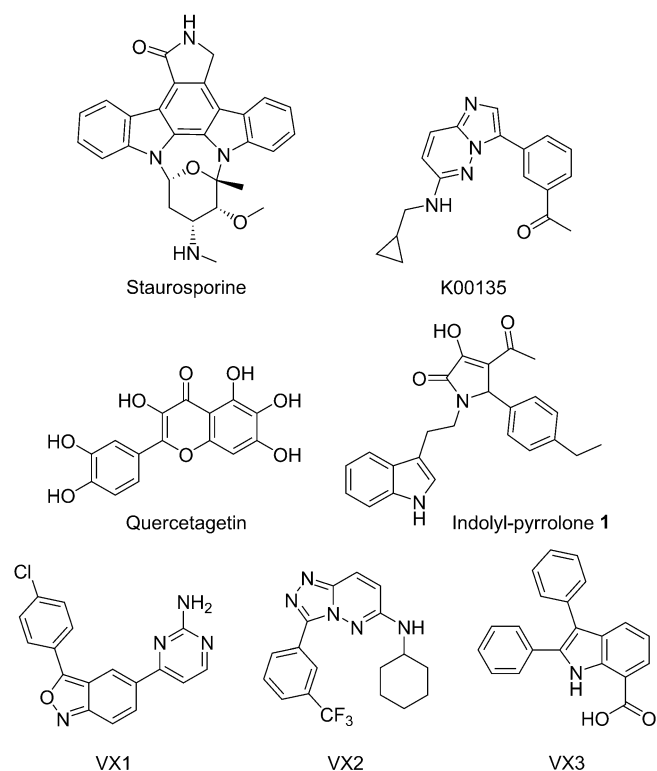


Figure 1. Examples of known Pim-1 inhibitors recently reported in the literature.

terized by a high degree of chemical diversity (Figure 1). These known inhibitors belong to different chemical classes, including ruthenium-containing organometallic complexes, bis-indolylmaleimides (e.g., staurosporine), imidazo[1,2-*b*]pyridazines (e.g., K00135), pyridones, flavonoids (e.g., quercetagenin), benzisoxazoles (e.g., VX1), isoxazolo[3,4-*b*]quinoline-diones, indolyl-pyrrolones, pyrrolo[2,3-*a*]carbazole, 3-*H*-benzo[4,5]thieno[3,2-*d*]pyrimidin-4-ones, thiazolidinediones, triazolo[4,3-*b*]pyridazines, triazolopyridazines (e.g., VX2), and dipheylindoles (e.g., VX3).^[13,14]

A key role in the discovery of novel Pim-1 inhibitors has been played by X-ray crystallography.^[5] Interestingly, crystal structures of Pim-1 have revealed an atypical sequence in the hinge region and a unique conformation that distinguishes this protein from other structurally related kinases. In detail, Pim-1 is characterized by the presence of a proline residue at position 123, thus the adenine nucleus of ATP cannot form the second hydrogen bond with the hinge region that is conserved in all other protein kinases. Because of the availability of many crystal structures, molecular modeling methods have been applied in recent years for the identification of Pim-1 inhibitors.^[15–20]

In this respect, a structure-based virtual screening approach was recently employed in our group by applying different filters such as pharmacophore models, drug-like property calculations, and docking simulations.^[16] As a result of this research, indolyl-pyrrolone 1 (Figure 1) emerged as a new scaffold and exhibited inhibitory activity in the micromolar range against Pim-1.^[16] Despite its peculiar structure, compound 1 is predict-

ed to adopt a canonical orientation within the binding site, being involved in the same putative pattern of interactions as staurosporine within the Pim-1 binding site.

Here, derivatives of 1 were synthesized based on molecular modeling studies and then assayed for their activity against Pim-1. A structure–activity relationship study of indolyl-pyrrolone Pim-1 inhibitors is reported. Furthermore, still pursuing the aim of identifying novel Pim-1 inhibitors, a structure-based drug design approach was applied that led to the identification of new hit compounds characterized by chemical scaffolds different to that of compound 1 as well as other Pim-1 inhibitors reported in literature. The approach described involved the use of a large amount of recently published crystallographic data that was not available during previous studies.^[16] Notably, two of the newly identified hit compounds showed an atypical mechanism of action, being noncompetitive against both ATP and the peptide substrate in enzymatic assays. This mechanism of action might be approximated as allosteric inhibition of Pim-1. To the best of our knowledge, no allosteric inhibitor of Pim-1 kinase has been reported so far, and as such, the results of this research lay the foundation for the development of noncompetitive Pim-1 inhibitors.

Compounds with significant inhibitory activity were also evaluated for their *in vitro* antitumoral effects against prostate cancer, for which Pim-1 is currently under investigation as a potential therapeutic target.^[21] Pim-1 inhibitors, at micromolar concentrations, decrease proliferation of different prostate cancer cells, and this effect was particularly evident in combination with the chemotherapeutic taxane, paclitaxel (PTX). Moreover a synergistic antiproliferative effect was observed in some cell lines when ATP-competitive and ATP noncompetitive compounds were used in combination.

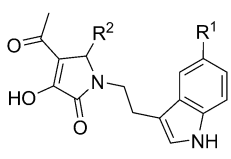
Results and Discussion

Indolyl-pyrrolone as a promising scaffold for Pim-1 inhibitors

In order to study the structure–activity relationships of indolyl-pyrrolones as Pim-1 inhibitors, a series of analogues (2–19) was synthesized and tested *in vitro* for their inhibitory activity against Pim-1 (Table 1). Taking into account the results from previous docking studies, modifications were introduced while maintaining the central core. In detail, our recent theoretical studies on indolyl-pyrrolone 1 highlighted the structural features responsible for the binding of this compound within the ATP binding site of Pim-1 kinase.^[16]

Compound 1 is predicted to bind with the indolyl-pyrrolone nucleus within the adenine region where it can engage in hydrogen bonds with Glu 121, Asp 128 and Val 126 (Figure 2a). Furthermore, hydrophobic contacts were predicted between the phenyl group of the ligand and Leu 44, Phe 49, Val 52, termed hydrophobic region I, and the indole ring and Val 52, Ala 65, Ile 104, Ile 185, termed hydrophobic region II. According with these considerations, we decided to synthesize: 1) derivatives bearing different hydrophobic substituents in the *para* or *meta* position of the phenyl ring in order to better explore the

Table 1. Structure and in vitro Pim-1 kinase inhibitory activities of compounds 2–19.^[a]



Compd	R ¹	R ²	ID ₅₀ [μM]	K _i [μM]
2	H	C ₆ H ₅	74	17.78
3	H	C ₆ H ₄ -4-Br	41	9.86
4	H	C ₆ H ₄ -4-CF ₃	68	16.35
5	H	C ₆ H ₄ -4-CH(CH ₃) ₂	20	4.81
6	H	C ₆ H ₄ -4-piperidin-1-yl	10	2.40
7	H	C ₆ H ₄ -4-C ₆ H ₅	18	4.33
8	H	C ₆ H ₄ -3-OC ₆ H ₅	28	6.73
9	H	CH ₂ CH ₂ C ₆ H ₅	≥ 100	n.d.
10	OCH ₃	C ₆ H ₅	136	32.69
11	OCH ₃	C ₆ H ₄ -4-Br	60	14.42
12	OCH ₃	C ₆ H ₄ -4-CF ₃	115	27.64
13	OCH ₃	C ₆ H ₄ -4-CH(CH ₃) ₂	109	26.20
14	OCH ₃	C ₆ H ₄ -4-piperidin-1-yl	≥ 100	n.d.
15	OCH ₃	C ₆ H ₄ -4-C ₆ H ₅	21	5.05
16	OCH ₃	C ₆ H ₄ -3-OC ₆ H ₅	≥ 100	n.d.
17	OCH ₃	CH ₂ CH ₂ C ₆ H ₅	≥ 100	n.d.
18	OCH ₃	C ₆ H ₄ -4-CH ₃	33	7.93
19	OCH ₃	C ₆ H ₄ -4-OCH ₃	19	4.57

[a] Compounds exhibiting an ID₅₀ value significantly greater than 100 μM were not investigated further. Not determined (n.d.). Data are the mean of three independent experiments. Standard deviation (SD) was lower than 5%. ID₅₀: concentration of the inhibitor that reduced the in vitro activity of Pim-1 by 50% under the conditions described in the Experimental Section.

interactions with hydrophobic region I; 2) analogues with a methoxy substituent in position 5 of the indole ring to investigate the effect of an additional lipophilic group within hydrophobic region II.

The synthesis of compounds 2–19 was accomplished via a one-pot, three-components Biginelli-like condensation (Scheme 1). Presumably, the reaction mechanism includes the formation of a Schiff base from the aldehyde and the amine, followed by reaction with the enolic form of 2,4-dioxopentanoic acid ethyl ester to give the final product through an intramolecular ring closure.^[22]

A microwave (MW)-assisted organic synthesis approach was followed for the synthesis of these compounds, since MW conditions usually allow shorter reaction times than traditional methods. For the synthesis of compounds 2–5, 7–13 and 15–19, 2,4-dioxopentanoic acid ethyl ester (20), tryptamine (21 a) or 5-methoxytryptamine (21 b), and the appropriate aldehyde (22 a–i) were reacted in the presence of a basic catalyst under MW irradiation (Scheme 1 A; Entry 1, Table 2).

In contrast, despite several attempts, the MW-assisted synthesis of 4-piperidinyl derivatives 6 and 14 led to a mixture of decomposition products, preventing the use of this technique (Entries 5–7, Table 2). Therefore, these two compounds were synthesized via a conventional method (Scheme 1 B). 2,4-Dioxopentanoic acid ethyl ester (20), tryptamine (21 a) or 5-methoxytryptamine (21 b), and 4-piperidin-1-yl-benzaldehyde

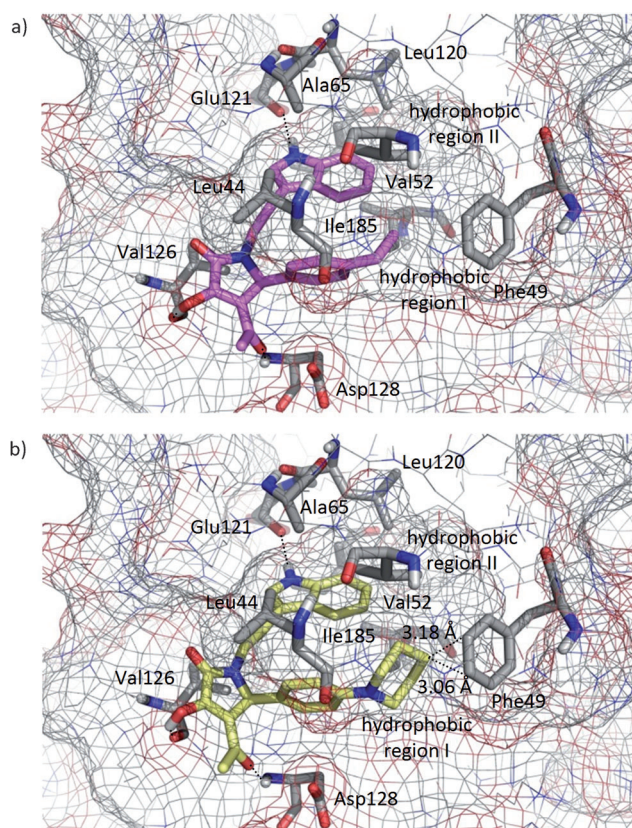


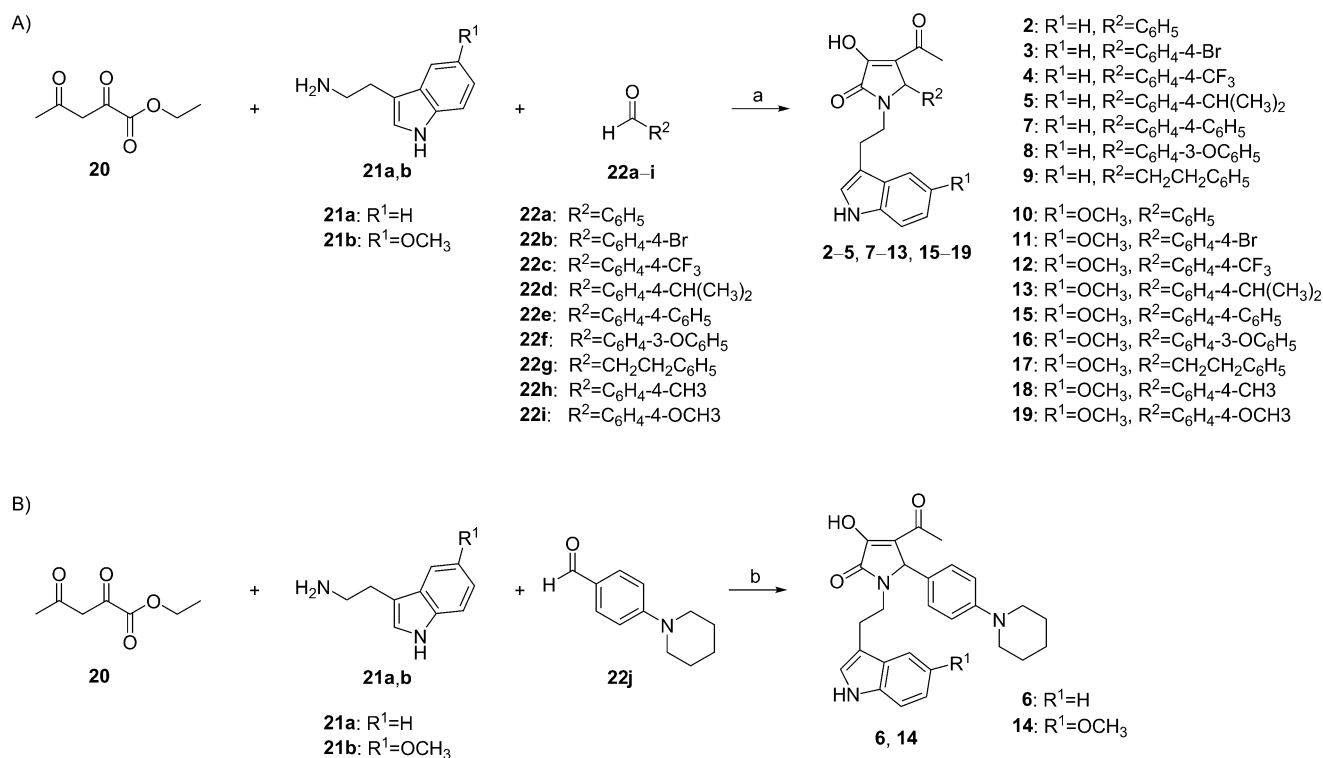
Figure 2. a) Predicted binding mode of the indolyl-pyrrolone 1. The new derivatives were designed in order to explore whether further hydrophobic interactions with hydrophobic regions I and II could influence the activity of the derivatives against Pim-1. b) Predicted binding mode of indolyl-pyrrolone 6.

(22 j) were reacted, in presence of a basic catalyst, at 80 °C for a significantly longer period (14 h) to obtain compounds 6 and 14 (Entry 8, Table 2).

Table 2. Preliminary study of synthesis optimization using compounds 4 and 6 as model systems.

Entry	Desired product	Catalyst ^[a]	Solvent ^[b]	Method ^[c]	20:21 a:22:cat ^[d]	Yield ^[e] [%]
1	4	DIPEA	DME	MW	1:1:1:0.1 ^[f]	39.6
2	4	AcOH	<i>i</i> PrOH	MW	1.25:1.23:1:17.5 ^[g]	30.0
3	4	AcOH	DME	MW	1:1:1:0.1	20.1
4	4	DIPEA	DME	Traditional	1:1:1:0.1	47.1
5	6	DIPEA	DME	MW	1:1:1:0.1	NP
6	6	AcOH	<i>i</i> PrOH	MW	1.25:1.23:1:17.5	NP
7	6	AcOH	DME	MW	1:1:1:0.1	NP
8	6	DIPEA	DME	Traditional	1:1:1:0.1	20.5
9	6	AcOH	<i>i</i> PrOH	Traditional	1.25:1.23:1:17.5	15.0

[a] *N,N*-Diisopropylethylamine (DIPEA) and acetic acid (AcOH) are indicated as catalysts even where used in excess. [b] Dimethoxyethane (DME), propan-2-ol (*i*PrOH). [c] Microwave (MW) conditions: 130 °C, 5 min, 300 W; traditional conditions: N₂ atmosphere, 80 °C, 14 h. [d] Ratio of reagents and catalyst (cat). Compound 22 refers to the appropriate derivative: i.e., 22 c for the synthesis of 4, and 22 j for the synthesis of 6. [e] Isolated yield of desired product. No product (NP) obtained. [f] Ratio selected according to experimental procedure reported by Zou et al.^[24] [g] Ratio selected according to experimental procedure reported by Choi et al.^[23]



Scheme 1. Synthesis of A) compounds 2–5, 7–13, 15–19, and B) compounds 6 and 14. Reagents and conditions: a) *N,N*-Diisopropylethylamine (DIPEA), dimethoxyethane (DME), microwave (300 W), 130 °C, 5 min, 15–69%; b) DIPEA, DME, 80 °C, 14 h, 21% (6) and 15% (14).

The evident difference in yield between MW and traditional synthesis for 4-piperidinyl derivatives prompted us to investigate whether the trend was maintained also for other compounds. 4-Trifluoromethyl derivative 4, which was obtained in fair yields using MW synthesis (40%), was resynthesized using a traditional protocol (Entry 4, Table 2). While the classical method led to a slight increase in yield (47%), comparison of the reaction times (5 min vs 14 h) indicated that MW irradiation is generally preferable for the synthesis of these compounds.

Since these reactions generally gave low yields, mainly due to the formation of several byproducts with a R_f values very similar to that of the desired compound, a preliminary study was conducted to evaluate the best reaction conditions. Starting from data reported in the literature, showing that analogues of these compounds have been synthesized both under acid and basic conditions,^[23,24] several experiments were performed in presence of acetic acid to verify the impact on the yields both in MW-assisted (Entries 2–3, Table 2) and traditional synthesis (Entry 9, Table 2). Data showed that basic catalysis gives the best results in both methods. Nevertheless, yields have to be further improved, and an optimization study is ongoing looking at other solvents and bases.

The synthesized compounds were assayed for their inhibitory activity toward Pim-1 (Table 1). With regard to compounds 2–8, the substitution of the hydrogen with bromine, trifluoromethyl, isopropyl, piperidine-*N*-yl and phenyl groups in the

para position of the phenyl ring, as well as the introduction of a methoxyphenyl moiety in the *meta* position, were favorable for activity. The best compounds in this series were 5–8 with ID₅₀ values of 20, 10, 18, 28 μM and K_i values of 4.81, 2.40, 4.33, 6.73 μM, respectively.

Conversely, the introduction of a methoxy group in position 5 of the indole ring (10–19) resulted to be detrimental to activity (cf. 10–14, 16 with 2–6, 8, respectively). Only compounds 15, 18, and 19, with ID₅₀ values of 21, 33, 19 μM and K_i values of 5.05, 7.93 and 4.57 μM, respectively, showed activities comparable with the best compounds of the unsubstituted series (5–8).

From docking studies, the proposed binding mode of the active compounds was comparable with that of the hit compound 1. Taken together, the results of the docking study and biological evaluation indicate that hydrophobic region I can accommodate both aliphatic and aromatic groups. For example, the predicted binding mode of compound 6, the most active indolyl-pyrrolone reported here, indicates that 6 establishes favorable CH–π interactions with the residue Phe49 (Figure 2b).

In contrast, placement of a methoxy group in hydrophobic region II is not favorable for activity. Despite the profitable hydrophobic interactions of the 5-methoxy group predicted to form within the pocket, a moderate loss of activity was observed for compounds 10–13 (cf. 2–5, respectively). This could be due to the energy cost required for the 5-substituted unbound ligand to achieve the predicted bound conformation in

solution. Indeed, we calculated that an energy cost of 13.05, 4.01, 2.67 and 4.63 kJ mol⁻¹ is required for compounds **10**, **11**, **12** and **13**, respectively, while the energy cost is approximately 0 kJ mol⁻¹ for binding of the 5-unsubstituted analogues **2–5** in the proposed conformation. On the other hand, a marked decrease in activity was observed for compounds **14** and **16** (cf. 5-unsubstituted derivatives **6** and **8**), which is probably due to steric hindrance caused by the R² substituent preventing the concurrent placement of the 5-methoxy group within the hydrophobic pocket.

Structure-based virtual screening

With the aim of identifying novel chemical scaffolds for Pim-1 inhibitors, with substantial chemical diversity in contrast to indolyl-pyrrolone **1**, a structure-based virtual screening relying on pharmacophore screening and molecular docking was performed. In contrast to the previous computational screening performed against Pim-1,^[16] at the time of the study described here, several additional crystallographic structures of Pim-1 in complex with ATP-competitive inhibitors were available (see Supporting Information). Crystallographic structures were classified into three groups based on the bound inhibitor scaffold, interaction pattern within the Pim-1 active site, and the conformation of the protein glycine-rich loop, which is also known as the P-loop.^[25]

Two main conformations of the P-loop were found in Pim-1 X-ray crystal structures, characterized by two different conformations of the Phe49 side chain: *P-loop-in*, where Phe49 points toward the hinge loop by partially occupying the adenylyl-imidodiphosphate (AMP-PNP) binding site; *P-loop-out*, where Phe49 points toward the solvent, and the loop adopts a more opened conformation.

Three main pharmacophores were generated for Pim-1/inhibitor complexes by using LigandScout 2.0,^[26] namely *pharm1* and *pharm2* accounting for the *P-loop-in* protein conformation and *pharm3* accounting for the *P-loop-out* conformation (see Supporting Information). These three pharmacophore models were then used as three-dimensional queries to screen the whole Asinex Ltd database (about 550 000 compounds). The FitValue was used as a measure of how well the ligand fits the pharmacophore. Accordingly, 8810 molecules mapping *pharm1* or *pharm2* with a FitValue higher than 2.0 and 699 molecules mapping *pharm3* with a FitValue higher than 3.5 were selected for subsequent docking studies.

Compounds filtered through the *pharm1* or *pharm2* pharmacophore models were docked toward the representative crystallographic structure of the Pim-1 catalytic site having a *P-loop-in* conformation (PDB: 2C3I).^[27] Conversely, compounds filtered through the *pharm3* model were docked with the Pim-1 catalytic site having a *P-loop-out* conformation (PDB: 1XR1).^[28] These structures were selected because they have the lowest root-mean-square deviation (RMSD) of active site atoms with respect to all other ligand-bound Pim-1 crystallographic structures available.^[29] A conserved crystallographic water molecule was retained and considered as part of the receptor. After protein relaxation by means of energy minimization, mo-

lecular docking was performed with GOLD by using the ChemScore function that was able to successfully self-dock crystallographic ligands into their native receptor structures. The docking-based binding modes of 500 top scoring compounds were visually analyzed, and molecules showing a similar interaction pattern within hydrophobic regions I and II were deemed top priority.

Twenty of the most interesting compounds (**23–42**) having a reasonable chemical diversity against known Pim-1 inhibitors were selected for further in vitro evaluations (for chemical structures, see the Supporting Information). Six compounds (**23**, **30**, **33**, **37**, **40** and **41**) were found to inhibit Pim-1 catalytic activity at concentrations lower than 100 μM in an enzymatic assay (Figure 3 and Table 3). Candidate hit compounds were subsequently tested by means of enzymatic and kinetic assays prior to being analyzed in prostate cancer (PC3) cells. In details, compounds were investigated for competition against ATP or peptide substrate, in order to elucidate the mechanism of inhibition. Curiously, while most hit compounds showed ATP and peptide substrates competition, 2-aminothiazole **37** was non-competitive either against the ATP or the peptide substrate.

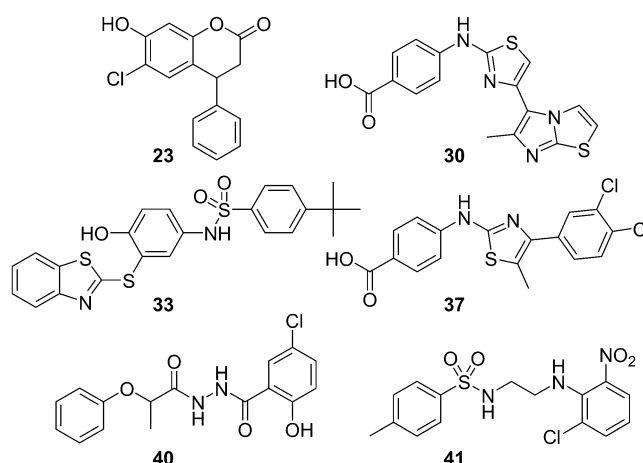


Figure 3. Of the twenty virtual hits evaluated, the six Pim-1 inhibitors shown here exhibited activity in an enzymatic assay. The full list of virtual hits **23–42** are given in the Supporting Information.

The 2-aminothiazole series

Allosteric sites on Pim-1 have not been hypothesized or identified yet. However, enzymatic assays and kinetic studies revealed that compound **37** inhibits Pim-1 by an atypical non-competitive mechanism that might be comparable with allosteric inhibition. With the aim of understanding possible molecular determinants responsible for the noncompetitive mechanism of inhibition, eight derivatives of **37** were purchased from Asinex Ltd and tested in vitro (Figure 4).

Compounds **43–50** exhibited a range of inhibitory activities against Pim-1, and most compounds were active at concentrations of less than 130 μM (Table 4). Compound **43** in particular showed the same mechanism of action already observed for

Compd	ID ₅₀ [μ M]	K _i [μ M]	Compd	ID ₅₀ [μ M]	K _i [μ M]
23	25.00	6.01	33	89.00	21.39
24	≥ 100	n.d.	34	≥ 100	n.d.
25	≥ 100	n.d.	35	≥ 100	n.d.
26	≥ 100	n.d.	36	≥ 100	n.d.
27	≥ 100	n.d.	37	10.00	10.00
28	≥ 100	n.d.	38	≥ 100	n.d.
29	≥ 100	n.d.	39	≥ 100	n.d.
30	8.55	2.05	40	12.54	3.01
31	≥ 100	n.d.	41	100.00	24.04
32	≥ 100	n.d.	42	≥ 100	n.d.

[a] Compounds exhibiting an ID₅₀ value significantly greater than 100 μ M were not investigated further. Not determined (n.d.). Data are the mean of three independent experiments. Standard deviation (SD) was lower than 5%.

37, being noncompetitive against ATP or the peptide substrate (Figure 5 and Table 5). Notably, compound **43** showed a greater potency than hit compound **37**. Interestingly, compound **43** was previously investigated as a Pim-1 inhibitor in the work of Pierce and coworkers, although they did not speculate on the possible mechanism of inhibition but rather pointed out that

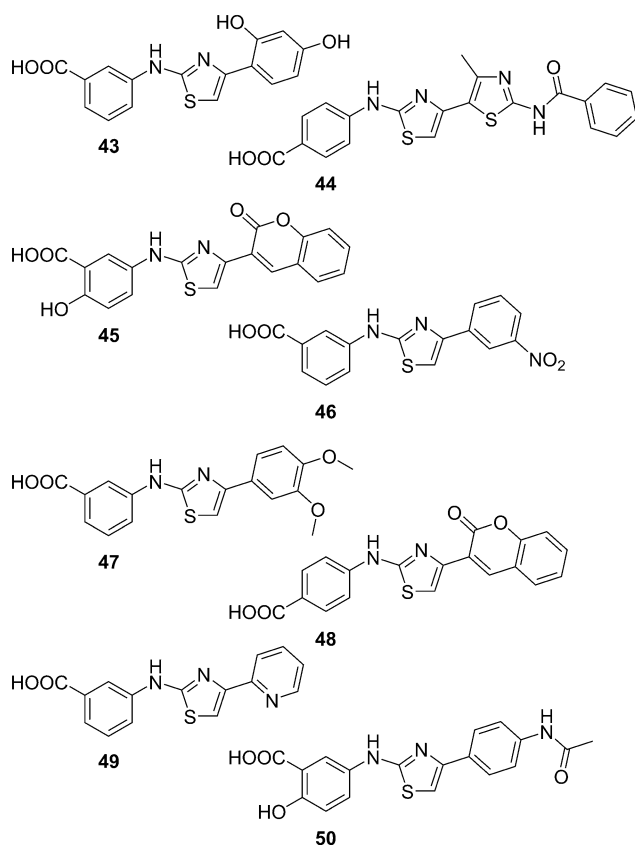


Figure 4. To gain insight into the structure–activity relationships and mechanism of inhibition of hit compound **37**, which exhibited good activity in vitro against Pim-1, the eight 2-aminothiazoles shown here were purchased from Asinex Ltd for further evaluation.

Compd	ID ₅₀ [μ M]	K _i [μ M]
43	2.65	2.65
44 ^[b]	5.00	1.20
45 ^[b]	26.80	6.44
46	111.00	n.d.
47	127.00	n.d.
48	207.00	n.d.
49	122.00	n.d.
50	206.00	n.d.

[a] Compounds exhibiting an ID₅₀ value of greater than 30 μ M were not investigated further. Not determined (n.d.). Data are the mean of three independent experiments. Standard deviation (SD) was lower than 5%.
[b] ATP-competitive.

co-crystallization of **43** within the catalytic active site by soaking was unsuccessful.^[17] Based on this evidence, studies aimed at the identification and characterization of the possible allosteric site of Pim-1 are currently going on.

Synergistic effects of drugs targeting catalytic and allosteric sites in the same enzyme have already been reported in the literature for nucleoside and non-nucleoside inhibitors of HIV-1 reverse transcriptase.^[30] To further confirm the noncompetitive mechanism of action of compound **43**, we investigated the in vitro effect of a combination of **43** with competitive Pim-1 inhibitors such as **40**, **6**, **1** and derivative **44**, which is structurally related to **43**. For each combination, the interaction index for 50% inhibition (I_{50}) value resulted lower than 1, thus indicating a synergistic effect between **43** with ATP-competitive inhibitors (Table 6). Combinations of ATP-competitive inhibitors **1** and **6**, as well as noncompetitive inhibitors **43** and **37**, were also performed, resulting in I_{50} values close to 1, which indicate a nonsynergistic effect, as expected for inhibitors that share the same mechanism of action.

Finally, based on the in vitro results, preliminary structure–activity relationship analysis for this series showed that molecular dimension might play a key role in discriminating between a noncompetitive and ATP-competitive mechanism of action. Noncompetitive inhibition was observed for the smallest 2-aminothiazoles (**37** and **43**), while those with bulkier substituents were competitive against both ATP and the peptide substrate. Phenolic hydroxy groups seem to improve the affinity of a ligand for Pim-1, probably due to the formation of additional hydrogen-bond contacts.

Cell culture assays

Over the last decade, increasing evidence has been accumulating regarding the potential role of Pim-1 as a prognostic marker in prostate cancer.^[31–33] For this reason, the development of effective Pim-1 inhibitors could have a great impact in the future therapy of prostate cancer. To further investigate the inhibition activity, as well as to probe their potential as anticancer agents, the most potent Pim-1 inhibitors described above were tested against a panel of prostate cancer cell lines: PC3, DU145, LNCaP and 22RV1.

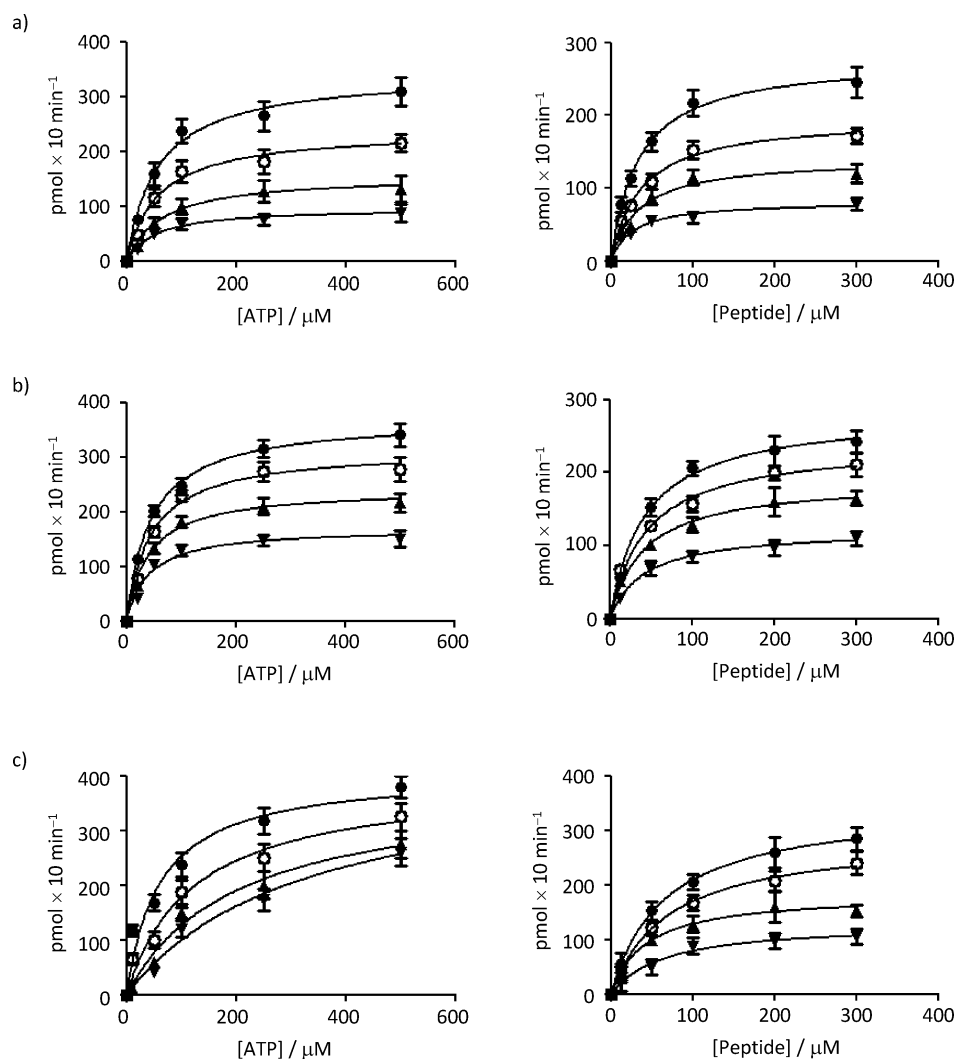


Figure 5. Kinetic analysis of kinase reactions of Pim-1 in the presence of different concentration of test compounds: a) **37** (●: 0 μM ; ○: 5 μM ; ▲: 10 μM ; ▼: 20 μM), b) **43** (●: 0 μM ; ○: 2 μM ; ▲: 3 μM ; ▼: 6 μM) and c) **6** (●: 0 μM ; ○: 5 μM ; ▲: 10 μM ; ▼: 20 μM). Left-hand side: Variation of the reaction velocity of Pim-1 as a function of ATP concentration at different fixed concentrations of test compound. Right-hand side: Variation of the reaction velocity of Pim-1 as a function of peptide substrate concentration at different fixed concentrations of test compound. Each reaction was performed as described in the Experimental Section; values are the mean of three independent experiments, and error bars represent \pm SD.

First, we evaluated the cytotoxicity of compounds **40**, **43** and **6** by determining the residual viability of cells treated for 48 hours and comparing the results against untreated control cells. Notably, all compounds exhibited an IC_{50} value below 50 μM in all cell lines (Table 7). Equimolar combination treatment with compounds **40** + **43** and **6** + **43** gave rise to an evident decrease in IC_{50} value, particularly for the **40** + **43** combination in PC3 and DU145 cells, when compared with treatment by the individual agents alone (Table 7). No synergistic effects were observed in the other cancer cell lines tested (DU145, LNCaP and 22RV1) when treated with the **43** + **6** combination (Table 7). Calculation of the combination index (CI) for the IC_{50} , IC_{75} and IC_{90} values further confirmed the synergistic effects of the **40** + **43** combination treatment in PC3 and DU145 cells (Table 8).

Pim-1 is mainly involved in promoting survival of cancer cells under apoptosis-inducing conditions, such as the presence of chemotherapeutic agents.^[31] For this reason, our compounds were also tested in combination with the well-known antitumor drug paclitaxel (PTX). This combination provided a more potent effect, especially for compound **40** that showed a 48% residual viability when treated at 10 μM in combination with PTX compared with a 80% residual viability when cells were treated with PTX alone (Figure 6). When we evaluated cell cycle distribution and apoptosis by flow cytometry, the synergistic effect was confirmed. In fact, the combination treatment **40** + PTX induced apoptosis in 31% of PC3 cells compared with 10% when treated with PTX alone. It is worth noting that these data are comparable with the percentage of apoptosis (~30%) observed under similar experimental conditions by silencing Pim-1 mRNA.^[31] Based on recent evidences about the role of Pim-1 in promoting cell survival under conditions of cellular stress and in response to taxanes, compounds **40**, **43**, and **6** could be promising adjuvant drugs for the treatment of prostate cancer and other malignancies in which Pim-1 is associated with chemotherapeutic resistance.

Conclusions

Pim-1 is a member of the serine/threonine kinase family, which is attracting much interest as drug targets for the pharmacological treatment of cancer. Despite evidence for the critical role of Pim-1 in the replication and survival of cancer cells, only a few molecules endowed with drug-like properties have been developed so far. In this work, we made a step forward in the characterization of Pim-1 inhibitors by expanding the indolyl-pyrrolone scaffold, already identified as an ATP-competitive Pim-1 inhibitor in a previous work.^[16]

In our search for chemically diverse Pim-1 inhibitors, we performed a virtual screening campaign that led to the identification of ATP-competitive inhibitors, as well as some 2-amino-

Table 5. Effect of compounds **37**, **43** and **6** at various concentrations (0–20 μM) on the K_m and V_{max} values.^[a]

Compd 37	Concentration			
	0 μM	5 μM	10 μM	20 μM
V_{max} (ATP) [$\mu\text{mol min}^{-1}$]	34.26 \pm 2.10	23.77 \pm 1.60	15.53 \pm 1.50	9.63 \pm 0.90
K_m (ATP) [μM]	48.23 \pm 4.10	48.75 \pm 3.80	48.11 \pm 3.80	50.01 \pm 4.20
V_{max} (peptide) [$\mu\text{mol min}^{-1}$]	27.75 \pm 1.28	19.60 \pm 0.99	14.00 \pm 0.66	8.15 \pm 0.62
K_m (peptide) [μM]	41.10 \pm 3.50	44.20 \pm 4.10	42.20 \pm 3.70	40.10 \pm 3.60
Compd 43	Concentration			
	0 μM	2 μM	3 μM	6 μM
V_{max} (ATP) [$\mu\text{mol min}^{-1}$]	36.95 \pm 1.30	31.40 \pm 1.50	24.11 \pm 1.10	16.95 \pm 0.80
K_m (ATP) [μM]	45.77 \pm 3.20	44.50 \pm 4.5	39.60 \pm 6.20	39.80 \pm 5.50
V_{max} (peptide) [$\mu\text{mol min}^{-1}$]	28.12 \pm 1.16	23.94 \pm 1.07	18.87 \pm 0.63	12.11 \pm 0.73
K_m (peptide) [μM]	43.20 \pm 4.10	45.60 \pm 3.50	45.40 \pm 3.70	44.80 \pm 3.90
Compd 6	Concentration			
	0 μM	5 μM	10 μM	20 μM
V_{max} (ATP) [$\mu\text{mol min}^{-1}$]	40.60 \pm 2.00	39.20 \pm 4.10	38.00 \pm 3.20	42.10 \pm 1.30
K_m (ATP) [μM]	55.47 \pm 5.70	115.10 \pm 11.8	199.10 \pm 15.40	299.40 \pm 25.70
V_{max} (peptide) [$\mu\text{mol min}^{-1}$]	34.20 \pm 1.70	28.10 \pm 1.60	18.20 \pm 0.87	12.90 \pm 1.07
K_m (peptide) [μM]	54.30 \pm 3.70	59.10 \pm 7.10	51.00 \pm 6.20	53.20 \pm 4.40

[a] Data represent the mean \pm standard deviation (SD) of three independent experiments.

Table 6. Synergistic interaction of **43** with compounds **40**, **6**, **1**, **44**.^[a]

Compd	I_{50}
43 + 40	0.50
43 + 6	0.59
43 + 1	0.74
43 + 44	0.76
43 + 37	0.92
6 + 1	0.99

[a] Interaction index for 50% inhibition (I_{50}) was calculated according to Equation (6). For full details, see the Experimental Section.

Table 7. Inhibitory activities of individual and combined compounds against prostate cancer cell lines.

Compd	IC_{50} [μM]			
	PC3	DU145	LNCaP	22RV1
6	34.0 \pm 2.3	26.3 \pm 1.6	41.0 \pm 5.5	32.6 \pm 4.3
40	21.0 \pm 3.4	22.4 \pm 3.2	20.8 \pm 3.3	14.4 \pm 3.2
43	30.4 \pm 2.7	47.3 \pm 6.5	27.5 \pm 2.5	32.6 \pm 3.4
40 + 43 ^[b]	12.1 \pm 4.1	10.6 \pm 6.2	13.8 \pm 3.3	15.3 \pm 4.5
6 + 43 ^[b]	14.1 \pm 3.7	37.7 \pm 5.4	54.6 \pm 4.6	26.0 \pm 3.5

[a] IC_{50} values were determined after 48 h incubation. Data represent the mean \pm standard deviation (SD) of three independent experiments.
[b] Compound combined in a 1:1 ratio.

Table 8. Combination index (CI) values calculated for the combination treatment of **40** + **43** corresponding to the IC_{50} , IC_{75} and IC_{90} values.

	CI (IC_{50})	CI (IC_{75})	CI (IC_{90})
PC3	0.79	0.76	0.82
DU145	0.56	0.47	0.41

thiazole derivatives endowed with a noncompetitive mechanism of Pim-1 inhibition. These compounds were classified as possible allosteric inhibitors, being noncompetitive with respect to both ATP and the peptide substrate. In vitro evaluation against recombinant Pim-1 confirmed the inhibitory activity of all hits identified in this work, and highlighted the synergistic effect of ATP-competitive inhibitors and 2-aminothiazole derivatives, when administered in combination.

In vitro assays performed in a number of human prostate cancer cell lines confirmed a broad activity against the different cell lines tested for representative compounds. In addition, the synergistic effect of a non-ATP competitive inhibitor was confirmed in more highly metastatic cell lines, PC3 and Du145, when used in combination with the most effective ATP-competitive compound.

In summary, we have presented a new series of valuable lead compounds with an ATP-competitive mechanism of action, and the 2-aminothiazole scaffold for noncompetitive, possibly allosteric, inhibitors of Pim-1. To the best of our knowledge, this is the first time that such a noncompetitive mechanism of inhibition has been declared for this serine/threonine kinase family member. In addition, since most potent Pim-1 inhibitors tested in PC3 cell lines showed a synergistic effect with paclitaxel, these derivatives could be promising adjuvant agents for the treatment of cancer diseases in which Pim-1 is associated with chemotherapeutic resistance.

Experimental Section

Computational methods

Molecular modeling studies on indolyl-pyrrolone derivatives: Docking studies of all indolyl-pyrrolone compounds were performed within the ATP binding site of Pim-1 (PDB: 1YHS)^[25] using the software package Gold version 4.1.^[34] Compounds were first processed with the Schrödinger LigPrep tool (version 25225) to generate separate files for all possible enantiomers and protonation states at physiological pH. Chemscore was chosen as the fitness function; the genetic algorithm parameter settings were employed using the search efficiency set at 100%, and 30 runs were carried out for each ligand. The compounds were docked exclusively as the enolic tautomer shown (as suggested by ¹H NMR analysis). Conformational search of compounds **2–5** and **10–13** was performed with the OPLS 2005 force field and using a GB/SA implicit solvent model.^[35–36]

Virtual screening: 37 crystallographic structures of Pim-1 in complex with inhibitors were downloaded from the Protein Data Bank (for a full list, see the Supporting Information). Common inhibitor scaffolds were analyzed and divided into three groups. A representative pharmacophore model was then generated for each group by LigandScout (version 3.0).^[26] Pharmacophore models were then converted in a format compatible with Discovery Studio 2.5 (Accelrys), which was used to screen the whole Asinex Ltd databases (Gold, Platinum, Synergy, Emerald and LeadLike collections). The "Best Flexible" search routine was applied to screen the database.

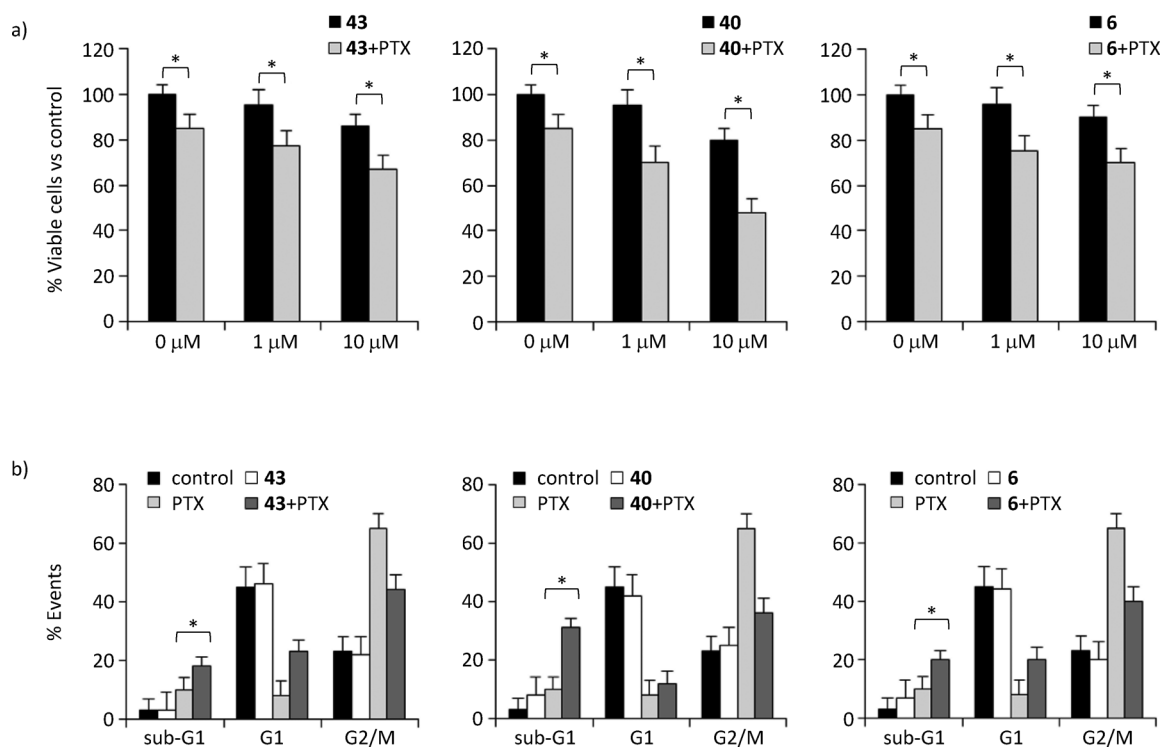


Figure 6. Prostate cancer cells (PC3) were treated with selected Pim-1 inhibitors in combination with paclitaxel (PTX). a) Residual viability of PC3 cells after treatment for 48 h with compounds **43**, **40** and **6** at 1 μM and 10 μM , and in combination with PTX (0.1 μM). b) Evaluation by flow cytometry of the proportion (%) of apoptotic cells (sub-G1) and cell cycle distribution in PC3 cells treated for 48 h with compounds **43**, **40** and **6** at 10 μM , and in combination with PTX (0.1 μM). Data represent the mean percentage of three different experiments with SD shown. * $P < 0.05$ according to a Student's t-test.

Conformational ensembles were generated with an energy threshold of 20 kcal mol⁻¹ from the local minimized structure, and a maximum limit of 255 conformers per molecule. The "Search 3D Database" protocol was used for mapping ligands to pharmacophores, whereas the "Ligand Pharmacophore Mapping" protocol was used to align selected ligands to the query pharmacophore and for calculating the relative FitValue.

PDB crystallographic structures 2C3I^[27] and 1XR1^[28] were selected for docking and prepared by means of the "Protein Preparation Wizard" implemented in MAESTRO 9.0.^[37] The protonation and tautomerization states of the residues were assigned for pH 7.0 \pm 1.0. Protein-ligand complexes were subjected to energy minimization using the OPLS-2005 force field until geometric convergence was achieved (RMSD = 0.3 Å).^[36]

The GOLD 4.1 docking program was chosen to perform automatic docking simulation of selected compounds and to evaluate the interaction energy between such compounds and the enzyme.^[38] The ChemScore function was used with default settings. The binding site was centered on the crystallographic ligand and had a radius of 10 Å.

Molecules selected by virtual screening were purchased from Asinex Ltd. The purity of the purchased molecules was reported by Asinex Ltd to range from 93 to 99%. To check this, we performed a HPLC analysis of compounds after shipping and storage, and we found the purities (92–98%) to be comparable to those reported by Asinex Ltd. ¹H NMR spectra were provided by Asinex Ltd, further confirming the purity of the samples and the structures of the compounds. The structures of all compounds purchased from Asinex Ltd are shown in the Supporting Information.

Chemistry

All commercially available reagents were purchased from Sigma-Aldrich and were used as received. Anhydrous reactions were run under a positive pressure of dry N₂. Flash chromatography was performed on columns packed with Merck silica gel 60, 23–400 mesh. Thin-layer chromatography (TLC) was carried out using Merck TLC silica gel 60 F254 plates. Melting points (mp) were determined with a Büchi 530 apparatus and are uncorrected. ¹H NMR spectra were recorded at 400 MHz in [D₆]DMSO on a Bruker Avance DPX400 spectrometer. Chemical shifts (δ) are reported in parts per million (ppm) relative to tetramethylsilane (TMS) as the internal standard. Coupling constants (J) are reported in Hz, and splitting patterns are described using the following abbreviations: singlet (s), doublet (d), triplet (t), quartet (q), quintet (quint), sextet (sx), multiplet (m), and broad (br). IR spectra were recorded on Perkin-Elmer 398 spectrophotometer using KBr pellets. Mass spectrometry (MS) data were obtained with an Agilent 1100 LC/MSD VL system (G1946C) at a flow rate of 0.4 mL min⁻¹ using a binary solvent system of MeOH/H₂O (95:5). Data were acquired using electrospray ionization (ESI) in the positive mode, scanning over the mass range 50–1500. UV detection was monitored at 254 nm, and the following ion source parameters were used: drying gas flow = 9 mL min⁻¹; nebulizer pressure = 40 psig; drying gas temperature = 350 °C. All target compounds possessed a purity of \geq 95%, which was verified by elemental analyses through comparison with theoretical values. Elemental analyses (C, H, N) were performed in house using a Carlo Erba 1106 Elemental Analyzer, and data are within 0.4% of the theoretical values.

Microwave (MW) irradiation experiments: Microwave irradiation experiments were conducted with a CEM Discover Synthesis Unit

(CEM Corp., Matthews, NC, USA). The instrument consists of a continuous focused microwave power delivery system with operator-selectable power output (0–300 W). The temperature of the vessel contents was monitored with a calibrated infrared temperature control unit mounted under the reaction vessel. All experiments were performed with a stirring option, whereby the contents of the vessel are stirred by means of a rotating magnetic plate located below the floor of the microwave cavity and a Teflon-coated magnetic stir bar in the vessel.

General procedure for the synthesis of 5-substituted derivatives 2–5, 7–13 and 15–19: A solution of **20** (100.0 mg, 0.630 mmol) in DME (4 mL) was treated with appropriate derivative **21** (0.630 mmol), appropriate aldehyde **22a–i** (0.630 mmol), and DIPEA (8.2 mg, 0.063 mmol), and the mixture was stirred at 130 °C under microwave irradiation (300 W) for 5 min. After cooling, EtOAc (5 mL) was added, and the solution was washed with saturated aq NH₄Cl (5 mL), water (5 mL), and brine (5 mL), then dried (MgSO₄), filtered and concentrated in vacuo. For products **2**, **4** and **9**, the compound was purified by crystallization from CH₂Cl₂/*n*-hexane (1:4). For products **3**, **5**, **7**, **8**, **10–13** and **15–19**, the compounds were first purified by column chromatography with gradient elution (CH₂Cl₂/MeOH/Et₃N, 100:0:0→95:5:1), and then recrystallized from CH₂Cl₂/*n*-hexane (1:4).

4-Acetyl-3-hydroxy-1-[2-(1H-indol-3-yl)ethyl]-5-phenyl-1,5-dihydro-2H-pyrrol-2-one (2): yellow–brown solid (157 mg, 69.3%); mp: 189–190 °C; ¹H NMR (400 MHz, [D₆]DMSO): δ = 2.01 (s, 3H, COCH₃), 2.70–2.92 (m, 4H, CH₂CH₂), 3.63–3.70 (m, 1H, CH), 5.00 (br s, 1H, NH, disappears with D₂O), 6.82–6.84 (m, 1H, indole H-2), 6.86–6.95 (m, 3H, Ar-H), 7.06–7.07 (m, 3H, Ar-H), 7.18–7.24 (m, 3H, Ar-H), 10.69 ppm (br s, 1H, OH, disappears with D₂O); IR (KBr): $\tilde{\nu}$ = 3455–3000 (OH), 3398 (NH), 1660 (CO), 1648 cm⁻¹ (CON); MS (ESI⁺): *m/z* 361 [M+H]⁺; Anal. calcd for C₂₂H₂₀N₂O₃: C 73.32, H 5.59, N 7.77, found: C 73.11, H 5.43, N 7.52.

4-Acetyl-5-(4-bromophenyl)-3-hydroxy-1-[2-(1H-indol-3-yl)ethyl]-1,5-dihydro-2H-pyrrol-2-one (3): brown–orange solid (53 mg, 19.0%); mp: 192–194 °C; ¹H NMR (400 MHz, [D₆]DMSO): δ = 1.97 (s, 3H, COCH₃), 2.57–2.83 (m, 4H, CH₂CH₂), 3.63–3.71 (m, 1H, CH), 5.89 (br s, 1H, NH, disappears with D₂O), 6.82–6.87 (m, 1H, indole H-2), 6.94–7.01 (m, 3H, Ar-H), 7.22–7.24 (m, 3H, Ar-H), 7.36–7.38 (m, 2H, Ar-H), 10.70 ppm (br s, 1H, OH, disappears with D₂O); IR (KBr): $\tilde{\nu}$ = 3450–3100 (OH), 3401 (NH), 1665 (CO), 1643 cm⁻¹ (CON); MS (ESI⁺): *m/z* 440 [M+H]⁺; Anal. calcd for C₂₂H₁₉BrN₂O₃: C 60.15, H 4.36, N 6.38, found: C 60.41, H 4.38, N 6.42.

4-Acetyl-3-hydroxy-1-[2-(1H-indol-3-yl)ethyl]-5-[4-(trifluoromethyl)phenyl]-1,5-dihydro-2H-pyrrol-2-one (4): yellow–brown solid (107 mg, 39.6%); mp: 220–225 °C; ¹H NMR (400 MHz, [D₆]DMSO): δ = 1.20 (s, 3H, COCH₃), 2.79–3.01 (m, 4H, CH₂CH₂), 3.80–3.85 (m, 1H, CH), 6.86–6.92 (m, 1H, indole H-2), 7.00–7.05 (m, 3H, Ar-H), 7.21–7.29 (m, 3H, Ar-H), 7.43–7.45 ppm (m, 2H, Ar-H); IR (KBr): $\tilde{\nu}$ = 3427 (NH), 3105 (OH), 1682 (CO), 1638 cm⁻¹ (CON); MS (ESI⁺): *m/z* 429 [M+H]⁺; Anal. calcd for C₂₃H₁₉F₃N₂O₃: C 64.48, H 4.47, N 6.54, found: C 64.80, H 4.32, N 6.84.

4-Acetyl-3-hydroxy-1-[2-(1H-indol-3-yl)ethyl]-5-(4-isopropylphenyl)-1,5-dihydro-2H-pyrrol-2-one (5): brown–orange solid (69 mg, 27.3%); mp: 188–191 °C; ¹H NMR (400 MHz, [D₆]DMSO): δ = 1.10–1.13 (m, 6H, 2CH₃ isoprop), 2.05 (s, 3H, COCH₃), 2.54–2.62 (m, 1H, CH isoprop), 2.79–2.88 (m, 4H, CH₂CH₂), 3.63–3.70 (m, 1H, CH), 5.00 (br s, 1H, NH, disappears with D₂O), 6.84–6.86 (m, 1H, indole H-2), 6.89–6.93 (m, 4H, Ar-H), 6.95–6.98 (m, 4H, Ar-H), 10.73 ppm (br s, 1H, OH, disappears with D₂O); IR (KBr): $\tilde{\nu}$ = 3400–3090 (OH), 3392 (NH), 1668 (CO), 1653 cm⁻¹ (CON); MS (ESI⁺): *m/z* 403 [M+

H]⁺; Anal. calcd for C₂₅H₂₆N₂O₃: C 74.60, H 6.51, N 6.96, found: C 74.42, H 6.67, N 7.09.

4-Acetyl-5-(1,1'-biphenyl-4-yl)-3-hydroxy-1-[2-(1H-indol-3-yl)ethyl]-1,5-dihydro-2H-pyrrol-2-one (7): brown–orange solid (59 mg, 21.6%); mp: 203–206 °C; ¹H NMR (400 MHz, [D₆]DMSO): δ = 2.00 (s, 3H, COCH₃), 2.79–2.90 (m, 4H, CH₂CH₂), 3.70 (m, 1H, CH), 5.10 (br s, 1H, NH, disappears with D₂O), 6.79–6.83 (m, 1H, indole H-2), 6.93–7.00 (m, 4H, Ar-H), 7.18–7.34 (m, 5H, Ar-H), 7.51–7.59 (m, 4H, Ar-H), 10.71 ppm (br s, 1H, OH, disappears with D₂O); IR (KBr): $\tilde{\nu}$ = 3405–3020 (OH), 3387 (NH), 1662 (CO), 1638 cm⁻¹ (CON); MS (ESI⁺): *m/z* 438 [M+H]⁺; Anal. calcd for C₂₈H₂₄N₂O₃: C 77.04, H 5.54, N 6.42, found: C 77.10, H 5.67, N 6.59.

4-Acetyl-3-hydroxy-1-[2-(1H-indol-3-yl)ethyl]-5-(3-phenoxyphenyl)-1,5-dihydro-2H-pyrrol-2-one (8): brown–orange solid (116 mg, 40.7%); mp: 205–208 °C; ¹H NMR (400 MHz, [D₆]DMSO): δ = 2.00 (s, 3H, COCH₃), 2.50–2.80 (m, 4H, CH₂CH₂), 3.65 (m, 1H, CH), 4.97 (br s, 1H, NH, disappears with D₂O), 6.76–6.81 (m, 1H, indole H-2), 6.83–6.87 (m, 4H, Ar-H), 6.94–7.03 (m, 5H, Ar-H), 7.22–7.26 (m, 4H, Ar-H), 10.71 ppm (br s, 1H, OH, disappears with D₂O); IR (KBr): $\tilde{\nu}$ = 3380–3000 (OH), 3385 (NH), 1667 (CO), 1641 cm⁻¹ (CON); MS (ESI⁺): *m/z* 454 [M+H]⁺; Anal. calcd for C₂₈H₂₄N₂O₄: C 74.32, H 5.35, N 6.19, found: C 74.50, H 5.71, N 6.47.

4-Acetyl-3-hydroxy-1-[2-(1H-indol-3-yl)ethyl]-5-(2-phenylethyl)-1,5-dihydro-2H-pyrrol-2-one (9): yellow–brown solid (127 mg, 59.7%); mp: 193–196 °C; ¹H NMR (400 MHz, [D₆]DMSO): δ = 1.80 (t, *J* = 6.2 Hz, 2H, CH₂CH₂C₆H₅), 2.10 (t, *J* = 6.2 Hz, 2H, CH₂CH₂C₆H₅), 2.18 (s, 3H, COCH₃), 2.78–2.84 (m, 2H, NCH₂CH₂), 2.93–2.95 (m, 2H, NCH₂CH₂), 3.84–3.91 (m, 1H, CH), 4.27 (br s, 1H, NH, disappears with D₂O), 6.86–6.90 (m, 1H, indole H-2), 6.96–7.05 (m, 3H, Ar-H), 7.11–7.26 (m, 3H, Ar-H), 7.46–7.48 (m, 3H, Ar-H), 10.80 ppm (br s, 1H, OH disappears with D₂O); IR (KBr): $\tilde{\nu}$ = 3390–3010 (OH), 3397 (NH), 1665 (CO), 1643 cm⁻¹ (CON); MS (ESI⁺): *m/z* 339 [M+H]⁺; Anal. calcd for C₂₄H₂₄N₂O₃: C 74.21, H 6.23, N 7.21, found: C 74.07, H 5.98, N 7.10.

4-Acetyl-3-hydroxy-1-[2-(5-methoxy-1H-indol-3-yl)ethyl]-5-phenyl-1,5-dihydro-2H-pyrrol-2-one (10): brown–orange solid (47 mg, 15.3%); mp: 192–196 °C; ¹H NMR (400 MHz, [D₆]DMSO): δ = 1.95 (s, 3H, COCH₃), 2.56–2.81 (m, 4H, CH₂CH₂), 3.64 (s, 3H, OCH₃), 3.70–3.72 (m, 1H, CH), 6.59–6.60 (m, 1H, indole H-2), 6.61–6.62 (m, 2H, Ar-H), 6.72–6.94 (m, 3H, Ar-H), 7.11–7.20 (m, 3H, Ar-H), 10.56 ppm (s, 1H, OH, disappears with D₂O); IR (KBr): $\tilde{\nu}$ = 3425–3000 (OH+NH), 1665 (CO), 1651 cm⁻¹ (CON); MS (ESI⁺): *m/z* 491 [M+H]⁺; Anal. calcd for C₂₃H₂₂N₂O₄: C 70.75, H 5.68, N 7.17, found: C 70.86, H 5.91, N 7.11.

4-Acetyl-5-(4-bromophenyl)-3-hydroxy-1-[2-(5-methoxy-1H-indol-3-yl)ethyl]-1,5-dihydro-2H-pyrrol-2-one (11): brown–orange solid (64 mg, 21.9%); mp: 196–198 °C; ¹H NMR (400 MHz, [D₆]DMSO): δ = 1.91 (s, 3H, COCH₃), 2.56–2.83 (m, 4H, 2CH₂), 3.63 (s, 3H, OCH₃), 3.70–3.74 (m, 1H, CH), 5.05 (br s, 1H, NH, disappears with D₂O), 6.60–6.62 (m, 1H, indole H-2), 6.70–6.95 (m, 3H, Ar-H), 7.03–7.13 (m, 2H, Ar-H), 7.35–7.38 (m, 2H, Ar-H), 10.58 ppm (s, 1H, OH, disappears with D₂O); IR (KBr): $\tilde{\nu}$ = 3340–3005 (OH+NH), 1684 (CO), 1642 cm⁻¹ (CON); MS (ESI⁺): *m/z* 470 [M+H]⁺; Anal. calcd for C₂₃H₂₁N₂O₄Br: C 58.86, H 4.52, N 5.97, found: C 58.73, H 4.76, N 5.67.

4-Acetyl-3-hydroxy-1-[2-(5-methoxy-1H-indol-3-yl)ethyl]-5-[4-(trifluoromethyl)phenyl]-1,5-dihydro-2H-pyrrol-2-one (12): brown–orange solid (76 mg, 26.3%); mp: 228–232 °C; ¹H NMR (400 MHz, [D₆]DMSO): δ = 1.99 (s, 3H, COCH₃), 2.56–2.82 (m, 4H, 2CH₂), 3.60 (s, 3H, OCH₃), 3.71 (m, 1H, CH), 5.09 (br s, 1H, NH, disappears with

D₂O), 6.68–6.72 (m, 1H, indole H-2), 6.95–7.13 (m, 3H, Ar-H), 7.24–7.26 (m, 2H, Ar-H), 7.51–7.52 (m, 2H, Ar-H), 10.55 ppm (s, 1H, OH, disappears with D₂O); IR (KBr): $\tilde{\nu}$ = 3400–3080 (OH+NH), 1678 (CO), 1635 cm⁻¹ (CON); MS (ESI+): *m/z* 459 [M+H]⁺; Anal. calcd for C₂₄H₂₁N₂O₄F₃: C 62.88, H 4.62, N 6.11, found: C 62.77, H 4.77, N 5.98.

4-Acetyl-3-hydroxy-5-(4-isopropylphenyl)-1-[2-(5-methoxy-1H-indol-3-yl)ethyl]-1,5-dihydro-2H-pyrrol-2-one (13): brown–orange solid (41 mg, 15.0%); mp: 194–196 °C; ¹H NMR (400 MHz, [D₆]DMSO): δ = 1.07–1.09 (m, 6H, 2CH₃ isoprop), 1.48–1.52 (m, 1H, CH isoprop), 1.90 (s, 3H, COCH₃), 2.55–2.75 (m, 4H, 2CH₂), 3.64 (s, 3H, OCH₃), 4.04–4.06 (m, 1H, CH), 5.02 (br s, 1H, NH, disappears with D₂O), 6.60–6.74 (m, 1H, indole H-2), 6.94–7.01 (m, 3H, Ar-H), 7.05–7.13 (m, 2H, Ar-H), 7.59–7.62 (m, 2H, Ar-H), 10.55 ppm (s, 1H, OH, disappears with D₂O); IR (KBr): $\tilde{\nu}$ = 3400–3000 (OH+NH), 1684 (CO), 1651 cm⁻¹ (CON); MS (ESI+): *m/z* 434 [M+H]⁺; Anal. calcd for C₂₆H₂₈N₂O₄: C 72.20, H 6.53, N 6.48, found: C 72.48, H 6.81, N 6.39.

4-Acetyl-5-(1,1'-biphenyl-4-yl)-3-hydroxy-1-[2-(5-methoxy-1H-indol-3-yl)ethyl]-1,5-dihydro-2H-pyrrol-2-one (15): brown–orange solid (74 mg, 25.0%); mp: 207–210 °C; ¹H NMR (400 MHz, [D₆]DMSO): δ = 1.90 (s, 3H, COCH₃), 2.42–2.88 (m, 4H, 2CH₂), 3.58 (s, 3H, OCH₃), 3.69–3.71 (m, 1H, CH), 5.10 (br s, 1H, NH, disappears with D₂O), 6.59–6.63 (m, 1H, indole H-2), 6.97–7.19 (m, 4H, Ar-H), 7.24–7.34 (m, 4H, Ar-H), 7.36–7.51 (m, 4H, Ar-H), 10.59 ppm (s, 1H, OH, disappears with D₂O); IR (KBr): $\tilde{\nu}$ = 3425–3070 (OH+NH), 1678 (CO), 1631 cm⁻¹ (CON); MS (ESI+): *m/z* 468 [M+H]⁺; Anal. calcd for C₂₉H₂₆N₂O₄: C 74.66, H 5.62, N 6.00, found: C 74.51, H 5.91, N 5.84.

4-Acetyl-3-hydroxy-1-[2-(5-methoxy-1H-indol-3-yl)ethyl]-5-(3-phenoxyphenyl)-1,5-dihydro-2H-pyrrol-2-one (16): brown–orange solid (46 mg, 15.1%); mp: 214–217 °C; ¹H NMR (400 MHz, [D₆]DMSO): δ = 1.97 (s, 3H, COCH₃), 2.51–2.82 (m, 4H, 2CH₂), 3.63 (s, 3H, OCH₃), 3.67–3.69 (m, 1H, CH), 6.60–6.63 (m, 1H, indole H-2), 6.76–6.94 (m, 4H, Ar-H), 7.00–7.13 (m, 4H, Ar-H), 7.21–7.25 (m, 4H, Ar-H), 10.56 ppm (s, 1H, OH, disappears with D₂O); IR (KBr): $\tilde{\nu}$ = 3380–3050 (OH+NH), 1684 (CO), 1641 cm⁻¹ (CON); MS (ESI+): *m/z* 484 [M+H]⁺; Anal. calcd for C₂₉H₂₆N₂O₅: C 72.18, H 5.43, N 5.81, found: C 71.95, H 5.48, N 5.70.

4-Acetyl-3-hydroxy-1-[2-(5-methoxy-1H-indol-3-yl)ethyl]-5-(2-phenylethyl)-1,5-dihydro-2H-pyrrol-2-one (17): brown–orange solid (58 mg, 22.0%); mp: 200–203 °C; ¹H NMR (400 MHz, [D₆]DMSO): δ = 1.90–2.12 (m, 4H, CH₂CH₂C₆H₅), 2.20 (s, 3H, COCH₃), 2.66–2.96 (m, 4H, 2CH₂), 3.66 (s, 3H, OCH₃), 3.84–3.91 (m, 1H, CH), 6.58–6.64 (m, 1H, indole H-2), 6.80–6.98 (m, 3H, Ar-H), 7.04–7.14 (m, 3H, Ar-H), 7.18–7.23 (m, 2H, Ar-H), 10.57 ppm (br s, 1H, OH, disappears with D₂O); IR (KBr): $\tilde{\nu}$ = 3380–3000 (OH+NH), 1675 (CO), 1636 cm⁻¹ (CON); MS (ESI+): *m/z* 419 [M+H]⁺; Anal. calcd for C₂₅H₂₆N₂O₄: C 71.75, H 6.26, N 6.69, found: C 71.82, H 6.47, N 6.54.

4-Acetyl-3-hydroxy-1-[2-(5-methoxy-1H-indol-3-yl)ethyl]-5-(4-methylphenyl)-1,5-dihydro-2H-pyrrol-2-one (18): brown–orange solid (137 mg, 54.0%); mp: 200–201 °C; ¹H NMR (400 MHz, [D₆]DMSO): δ = 2.27 (s, 3H, C₆H₄-4-CH₃), 2.37 (s, 3H, COCH₃), 2.93–3.05 (m, 4H, 2CH₂), 3.85 (s, 3H, OCH₃), 4.23–4.37 (m, 1H, CH), 6.84–6.95 (m, 1H, indole H-2), 7.00–7.28 (m, 3H, Ar-H), 7.30–7.35 (m, 2H, Ar-H), 7.38–7.41 (m, 2H, Ar-H), 8.59 ppm (br s, 1H, OH, disappears with D₂O); IR (KBr): $\tilde{\nu}$ = 3390–3000 (OH), 3385 (NH), 1671 (CO), 1647 cm⁻¹ (CON); MS (ESI+): *m/z* 406 [M+H]⁺; Anal. calcd for C₂₄H₂₄N₂O₄: C 71.27, H 5.98, N 6.93, found: C 71.48, H 6.25, N 7.02.

4-Acetyl-3-hydroxy-1-[2-(5-methoxy-1H-indol-3-yl)ethyl]-5-(4-methoxyphenyl)-1,5-dihydro-2H-pyrrol-2-one (19): brown–orange solid (135 mg, 51.0%); mp: 198–199 °C; ¹H NMR (400 MHz, [D₆]DMSO): δ = 2.38 (s, 3H, COCH₃), 2.90–3.02 (m, 4H, 2CH₂), 3.75 (s, 3H, C₆H₄-4-OCH₃), 3.87 (s, 3H, OCH₃), 4.21–4.33 (m, 1H, CH), 6.78–6.93 (m, 1H, indole H-2), 7.00–7.17 (m, 3H, Ar-H), 7.18–7.26 (m, 2H, Ar-H), 7.29–7.36 (m, 2H, Ar-H), 8.58 ppm (br s, 1H, OH, disappears with D₂O); IR (KBr): $\tilde{\nu}$ = 3395–3000 (OH), 3382 (NH), 1675 (CO), 1652 cm⁻¹ (CON); MS (ESI+): *m/z* 422 [M+H]⁺; Anal. calcd for C₂₄H₂₄N₂O₅: C 68.56, H 5.75, N 6.66, found: C 68.49, H 5.77, N 6.81.

General procedure for the synthesis of derivatives 6 and 14: A solution of **20** (100.0 mg, 0.630 mmol) in DME (4 mL) was treated with appropriate derivative **21** (0.630 mmol), **22j** (118 mg, 0.630 mmol), and DIPEA (8.2 mg, 0.063 mmol), and the mixture was stirred for 14 h at 80 °C under a nitrogen atmosphere. After cooling, EtOAc (5 mL) was added, and the solution was washed with saturated aq NH₄Cl (5 mL), water (5 mL), brine (5 mL), then dried (MgSO₄), filtered and concentrated in vacuo. The crude material was first purified by column chromatography (silica gel 70–230 mesh) with gradient elution (CH₂Cl₂/MeOH/Et₃N, 100:0:0 → 95:5:1), and the resultant brown–orange solid was further purified by recrystallization from CH₂Cl₂/*n*-hexane (1:4).

4-Acetyl-3-hydroxy-1-[2-1H-indol-3-yl)ethyl]-5-(4-piperidin-1-yl-phenyl)-1,5-dihydro-2H-pyrrol-2-one (6): brown–orange solid (57 mg, 20.5%); mp: 195–199 °C; ¹H NMR (400 MHz, [D₆]DMSO): δ = 1.40–1.45 (m, 2H, CH₂ pip), 1.48–1.52 (m, 4H, 2CH₂ pip), 2.05 (s, 3H, COCH₃), 2.75–2.55 (m, 4H, CH₂CH₂), 2.95–3.00 (m, 4H, 2CH₂N pip), 3.60 (m, 1H, CH), 4.99 (br s, 1H, NH, disappears with D₂O), 6.75–6.83 (m, 1H, indole H-2), 6.85–6.89 (m, 3H, Ar-H), 6.94–6.98 (m, 3H, Ar-H), 7.21–7.23 (m, 2H, Ar-H), 10.69 ppm (br s, 1H, OH, disappears with D₂O); IR (KBr): $\tilde{\nu}$ = 3430–3080 (OH+NH), 1650 (CO), 1610 cm⁻¹ (CON); MS (ESI+): *m/z* 445 [M+H]⁺; Anal. calcd for C₂₇H₂₉N₃O₃: C 73.11, H 6.59, N 9.47, found: C 72.99, H 6.43, N 9.35.

4-Acetyl-3-hydroxy-1-[2-(5-methoxy-1H-indol-3-yl)ethyl]-5-(4-piperidin-1-ylphenyl)-1,5-dihydro-2H-pyrrol-2-one (14): brown–orange solid (46 mg, 15.3%); mp: 203–207 °C; ¹H NMR (400 MHz, [D₆]DMSO): δ = 1.40–1.47 (6H, 3CH₂ pip), 1.85 (s, 3H, COCH₃), 2.75–2.95 (m, 8H, 2CH₂+2CH₂N pip), 3.63 (s, 3H, OCH₃), 3.70–3.72 (m, 1H, CH), 6.60–6.62 (m, 1H, indole H-2), 6.72–6.78 (m, 3H, Ar-H), 6.92–6.98 (m, 2H, Ar-H), 7.11–7.13 (m, 2H, Ar-H), 10.57 ppm (br s, 1H, OH, disappears with D₂O); IR (KBr): $\tilde{\nu}$ = 3420–3040 (OH+NH), 1682 (CO), 1637 cm⁻¹ (CON); MS (ESI+): *m/z* 475 [M+H]⁺; Anal. calcd for C₂₈H₃₁N₃O₄: C 71.01, H 6.60, N 8.87, found: C 70.88, H 6.72, N 8.74.

Biology

Cell culture and viability analysis: The biological activity of Pim-1 inhibitors was tested in human prostate cancer cell lines PC3, DU145, LNCaP and 22RV1. Cell lines were originally obtained from the American Type Culture Collection (ATCC) (Rockville, MD, USA). Cells were cultured according to the conditions indicated by the cell depository. Cell growth was analyzed by a cell counting assay. Prostate cancer cells were seeded onto six-well plates (1 × 10⁵ cells/well), and 24 h later, the medium was replaced with fresh medium (untreated control cultures) or medium containing test compound at the desired concentration. After 48 h incubation, cells were collected by trypsinization, centrifuged and resuspended in a known amount of culture medium. Aliquots of cell suspension were counted by a Neubauer hemocytometric chamber. Viability was as-

essed by the trypan blue dye exclusion test. IC₅₀ values and combination index (CI) data were calculated using the CalcuSyn software 2.1 (BioSoft, Cambridge, UK).

Flow cytometric analysis: The cell cycle progression and apoptosis was evaluated by flow cytometry according to standard procedures. Briefly, cells (1 × 10⁶) were washed with phosphate-buffered saline (PBS) and fixed for 30 min with 70% v/v EtOH at 4 °C. After washing with PBS, the cells were incubated in 1 mL of DNA staining solution (PBS containing 200 μg mL⁻¹ of RNase A, 20 μg mL⁻¹ of propidium iodide, and 0.1% v/v Triton X-100) at RT for 1 h. Suspended cells were analyzed on a FACScan instrument (Becton-Dickinson, Franklin Lakes, NJ, USA) using the Cell Quest software 3.1 (Becton-Dickinson). Analysis was performed by evaluating at least 10 000 cells for each sample. All measurements were performed using the same instrument settings. Apoptotic cells were detected by a quantifiable peak in sub-G1 phase corresponding to the red fluorescent light emitted by subdiploid cell nuclei.

Inhibition assay: Recombinant Pim-1 was purchased from Upstate (Millipore). Reactions were performed according to the manufacturer's protocol. Each compound was tested in the presence of 500 μM ATP and 100 μM peptide substrates (RBER-GSK3 14-27, Pro-Qinase) and in the presence of 0.01 μg active Pim-1, 0.33 pmol [³²P]ATP, 10 mM magnesium acetate, 8 mM 3-(*N*-morpholino)propanesulfonic acid (MOPS)/sodium hydroxide (pH 7), 1 mM ethylenediaminetetraacetic acid (EDTA), and 10% DMSO in a final volume of 10 μL. After 5 min at 30 °C, the reaction was stopped by adding 2 μL of 3% phosphoric acid. Aliquots (10 μL) were then transferred into a P30 Filtermat (PerkinElmer), washed five times with 75 mM phosphoric acid and once with acetone for 2 min. The filter was dried and transferred to a sealable plastic bag, and scintillation cocktail (4 mL) was added. Spotted reactions were read in a scintillation counter. The ID₅₀ values were obtained according to Equation (1), where *v* is the measured reaction velocity, *V* is the apparent maximal velocity in the absence of inhibitor, *I* is the inhibitor concentration, and the ID₅₀ is the 50% inhibitory dose.

$$v = V / (1 + (I/ID_{50})) \quad (1)$$

Inhibition mechanism: Pim-1 kinase activity assays were performed in the presence of different fixed amounts of inhibitor with varying substrate (ATP or peptide) concentrations. Data were analyzed according to the Michaelis-Menten method. *K_i* values, expressed as a concentration (μM), toward recombinant human Pim-1 were calculated according to Equation (2) for competitive inhibition toward ATP and peptide substrates, and Equation (3) for noncompetitive inhibition, where [S_{ATP}] and [S_{pep}] are the concentration of competing substrate (ATP and peptide, respectively). Each experiment was performed in triplicate, and mean values were used for interpolation. Curve fitting was performed with the program GraphPad Prism 5.00.

$$K_i = (ID_{50} / (1 + K_{mATP} / [S_{ATP}])) / (1 + K_{mpep} / [S_{pep}]) \quad (2)$$

$$K_i = ID_{50} \quad (3)$$

Determination of synergy: Analysis of the interaction between two inhibitors was performed according to the null reference mode of Loewe additivity.^[39] Dose-response curves for the interaction between two inhibitors were assumed to follow Hill's model and were generated by fitting the experimental data to Equation (4), where *E* is the observed effect (% activity), *E_{con}* is the control effect (activity in absence of inhibitor), *D₅₀* is the 50% inhibitory concentration, and *m* is a sigmoidicity parameter. From combinations of

two inhibitors at a fixed molar ratio (*R* = [inhibitor 1]/[inhibitor 2]), *D₁* and *D₂* values were calculated from the *D₅₀* value derived from Equation (4), with (*D₁* + *D₂*) = *D₅₀* and *D₁* = *R**D₂*.

$$E = (E_{con} ([I]/D_{50})^m) / (1 + (D_{50}/[I])^m) \quad (4)$$

Expected *D₁*, *D₂*, and *D_i* values for the combination of *i* drugs under the null reference hypothesis of no interaction were derived by inserting estimated *D₅₀* and *m* values for each drug in the combination in the specific form of the Lowe additivity equation [Eq. (5)], which assumes that Equation (4) is appropriate for each drug individually.^[39]

$$1 = (D_1 / (D_{50(1)} (E / (E_{con} - E))^{1/m_1})) + (D_2 / (D_{50(2)} (E / (E_{con} - E))^{1/m_2})) + \dots + (D_i / (D_{50(i)} (E / (E_{con} - E))^{1/m_i})) \quad (5)$$

The interaction index (*I*) was then calculated according to Berenbaum using Equation (6), where *D₁* and *D₂* are the concentrations of the drugs giving 50% inhibition when tested in the combination *D₁* + *D₂*, and *D₅₀₍₁₎* and *D₅₀₍₂₎* are the concentrations of each drug giving 50% inhibition when tested individually. A value for *I* < 1 indicates synergy, *I* > 1 indicates antagonism, and *I* = 1 indicates additivity, according to the Lowe additivity model. The null reference hypothesis of no interaction [Eq. (6)] corresponded to *I* = 1.

$$I = D_{(1)} / D_{50(1)} + D_{(2)} / D_{50(2)} \quad (6)$$

All of the analyses are based on the results of three independent experiments for each drug combination, and the standard deviation (SD) for each parameter estimate is indicated.

Acknowledgements

The authors thank the University of Siena (Italy) for support of the research presented here. This work has been partially supported by the Italian Cancer Research Association (AIRC) (grant no. IG12084) to G.M.

Keywords: cancer · medicinal chemistry · noncompetitive inhibition · Pim-1 · organic synthesis

- [1] H. T. Cuypers, G. Selten, W. Quint, M. Zijlstra, E. R. Maandag, W. Boelens, P. van Wezenbeek, C. Melief, A. Berns, *Cell* **1984**, *37*, 141–150.
- [2] N. M. van der Lugt, J. Domen, E. Verhoeven, K. Linders, H. van der Gulden, J. Allen, A. Berns, *EMBO J.* **1995**, *14*, 2536–2544.
- [3] B. K. Popivanova, Y. Y. Li, H. Zheng, K. Omura, C. Fujii, K. Tsuneyama, N. Mukaida, *Cancer Sci.* **2007**, *98*, 321–328.
- [4] A. L. Merkel, E. Meggers, M. Ocker, *Expert Opin. Invest. Drugs* **2012**, *21*, 425–436.
- [5] S. Schenone, C. Tintori, M. Botta, *Curr. Pharm. Des.* **2010**, *16*, 3964–3978.
- [6] Y. Alvarado, F. J. Giles, R. T. Swords, *Expert Rev. Hematol.* **2012**, *5*, 81–96.
- [7] L. Brault, C. Gasser, F. Bracher, K. Huber, S. Knapp, J. Schwaller, *Haematologica* **2010**, *95*, 1004–1015.
- [8] J. Kim, M. Roh, S. A. Abdulkadir, *BMC Cancer* **2010**, *10*, 248.
- [9] V. Magistroni, L. Mologni, S. Sanselicio, J. F. Reid, S. Redaelli, R. Piazza, M. Viltadi, G. Bovo, G. Strada, M. Grasso, M. Gariboldi, C. Gambacorti-Passerini, *PLoS One* **2011**, *6*, e28162.
- [10] J. Wang, P. D. Anderson, W. Luo, D. Gius, M. Roh, S. A. Abdulkadir, *Oncogene* **2012**, *31*, 1794–1803.
- [11] M. Zemskova, M. B. Lilly, Y. W. Lin, J. H. Song, A. S. Kraft, *Mol. Cancer Res.* **2010**, *8*, 1126–1141.

- [12] H. Akasaka, T. Akasaka, M. Kurata, C. Ueda, A. Shimizu, T. Uchiyama, H. Ohno, *Cancer Res.* **2000**, *60*, 2335–2341.
- [13] F. Anizon, A. A. Shtil, V. N. Danilenko, P. Moreau, *Curr. Med. Chem.* **2010**, *17*, 4114–4133.
- [14] T. Morwick, *Expert Opin. Ther. Pat.* **2010**, *20*, 193–212.
- [15] S. Doudou, R. Sharma, R. H. Henschman, D. W. Sheppard, N. A. Burton, *J. Chem. Inf. Model.* **2010**, *50*, 368–379.
- [16] S. Olla, F. Manetti, E. Crespan, G. Maga, A. Angelucci, S. Schenone, M. Bologna, M. Botta, *Bioorg. Med. Chem. Lett.* **2009**, *19*, 1512–1516.
- [17] A. C. Pierce, M. Jacobs, C. Stuver-Moody, *J. Med. Chem.* **2008**, *51*, 1972–1975.
- [18] F. Sliman, M. Blairvacq, E. Durieu, L. Meijer, J. Rodrigo, D. Desmaele, *Bioorg. Med. Chem. Lett.* **2010**, *20*, 2801–2805.
- [19] Y. Tong, K. D. Stewart, S. Thomas, M. Przytulinska, E. F. Johnson, V. Klinghofer, J. Levenson, O. McCall, N. B. Soni, Y. Luo, N. H. Lin, T. J. Sowin, V. L. Giranda, T. D. Penning, *Bioorg. Med. Chem. Lett.* **2008**, *18*, 5206–5208.
- [20] Z. Xia, C. Knaak, J. Ma, Z. M. Beharry, C. McInnes, W. Wang, A. S. Kraft, C. D. Smith, *J. Med. Chem.* **2009**, *52*, 74–86.
- [21] Y. Xie, K. Xu, D. E. Linn, X. Yang, Z. Guo, H. Shimelis, T. Nakanishi, D. D. Ross, H. Chen, L. Fazli, M. E. Gleave, Y. Qiu, *J. Biol. Chem.* **2008**, *283*, 3349–3356.
- [22] V. L. Gein, N. N. Kasimova, *Russ. J. Gen. Chem.* **2005**, *75*, 254–260.
- [23] S. Choi, A. Branstrom, S. A. Gothe, R. Lipman, N. Tamilarasu, R. G. Wilde, (PTC Therapeutics Inc., South Plainfield, USA), WO/2008/127275, **2008**.
- [24] D. Zou, H.-X. Zhai, J. Eckman, P. Higgins, M. Gillard, L. Knerr, S. Carre, P. Pasau, P. Collart, J. Grassi, *Letts. Drug Des. Discovery* **2007**, *4*, 185–191.
- [25] M. D. Jacobs, J. Black, O. Futer, L. Swenson, B. Hare, M. Fleming, K. Saxena, *J. Biol. Chem.* **2005**, *280*, 13728–13734.
- [26] G. Wolber, T. Langer, *J. Chem. Inf. Model.* **2005**, *45*, 160–169.
- [27] V. Pogacic, A. N. Bullock, O. Fedorov, P. Filippakopoulos, C. Gasser, A. Biondi, S. Meyer-Monard, S. Knapp, J. Schwaller, *Cancer Res.* **2007**, *67*, 6916–6924.
- [28] K. C. Qian, L. Wang, E. R. Hickey, J. Studts, K. Barringer, C. Peng, A. Kronkaitis, J. Li, A. White, S. Mische, B. Farmer, *J. Biol. Chem.* **2005**, *280*, 6130–6137.
- [29] D. Cappel, R. Wahlstrom, R. Brenk, C. A. Sotriffer, *J. Chem. Inf. Model.* **2011**, *51*, 2581–2594.
- [30] S. Yuasa, Y. Sadakata, H. Takashima, K. Sekiya, N. Inouye, M. Ubasawa, M. Baba, *Mol. Pharmacol.* **1993**, *44*, 895–900.
- [31] J. L. Hsu, P. K. Leong, Y. F. Ho, L. C. Hsu, P. H. Lu, C. S. Chen, J. H. Guh, *Cancer Lett.* **2012**, *319*, 214–222.
- [32] S. M. Dhanasekaran, T. R. Barrette, D. Ghosh, R. Shah, S. Varambally, K. Kurachi, K. J. Pienta, M. A. Rubin, A. M. Chinnaiyan, *Nature* **2001**, *412*, 822–826.
- [33] H. C. He, X. C. Bi, Z. W. Zheng, Q. S. Dai, Z. D. Han, Y. X. Liang, Y. K. Ye, G. H. Zeng, G. Zhu, W. D. Zhong, *Med. Oncol.* **2009**, *26*, 303–308.
- [34] M. L. Verdonk, J. C. Cole, M. J. Hartshorn, C. W. Murray, R. D. Taylor, *Proteins* **2003**, *52*, 609–623.
- [35] W. L. Jorgensen, D. S. Maxwell, J. TiradoRives, *J. Am. Chem. Soc.* **1996**, *118*, 11225–11236.
- [36] MacroModel version 9.9, Schrödinger, LLC, New York, NY, USA, **2011**.
- [37] Schrödinger Suite 2011: Protein Preparation Wizard; Epik version 2.2; Impact version 5.7; Prime version 3.0, Schrödinger, LLC, New York, NY, USA, **2011**.
- [38] G. Jones, P. Willett, R. C. Glen, A. R. Leach, R. Taylor, *J. Mol. Biol.* **1997**, *267*, 727–748.
- [39] W. R. Greco, G. Bravo, J. C. Parsons, *Pharmacol. Rev.* **1995**, *47*, 331–385.

Received: October 19, 2012